Chlorella-enriched hydrogels protect against myocardial damage and reactive oxygen species production in an *in vitro* ischemia/reperfusion model using cardiac spheroids

Biofabrication

PAPER

Chlorella-enriched hydrogels protect against myocardial damage and reactive oxygen species production in an *in vitro* ischemia/reperfusion model using cardiac spheroids

Martine Tarsitano[1,2], **Clara Liu Chung Ming**[1,3], **Lucia Bennar**[4], **Hadi Mahmodi**[5], **Kaitlin Wyllie**[6,7], **Dana Idais**[1,3], **Wafa Al Shamery**[1,3], **Donatella Paolino**[2,8], **Thomas R Cox**[6,7], **Irina Kabakova**[5], **Peter Ralph**[4] **and Carmine Gentile**[1,3,*]

[1] Faculty of Engineering and IT, University of Technology Sydney, Ultimo, NSW 2007, Australia
[2] Department of Experimental and Clinical Medicine, University 'Magna Graecia' of Catanzaro, Catanzaro 88100, Italy
[3] Heart Research Institute, Newtown, NSW 2042, Australia
[4] Climate Change Cluster, University of Technology Sydney, Ultimo, Sydney, NSW 2007, Australia
[5] School of Mathematical and Physical Sciences, University of Technology Sydney, Ultimo, NSW 2007, Australia
[6] The Garvan Institute of Medical Research and The Kinghorn Cancer Centre, Darlinghurst, NSW 2010, Australia
[7] School of Clinical Medicine, St Vincent's Healthcare Clinical Campus, UNSW Medicine and Health, Sydney, NSW 2052, Australia
[8] Research Center 'ProHealth Translational Hub', Department of Experimental and Clinical Medicine, 'Magna Graecia' University of Catanzaro, Catanzaro 88100, Italy
[*] Author to whom any correspondence should be addressed.

E-mail: Carmine.Gentile@uts.edu.au

OPEN ACCESS

RECEIVED
5 April 2024

REVISED
24 July 2024

ACCEPTED FOR PUBLICATION
2 October 2024

PUBLISHED
24 October 2024

Keywords: microalgae, hydrogels, cardiac spheroids, *in vitro* modelling, myocardial infarction, reactive oxygen species, Chlorella vulgaris

Supplementary material for this article is available online

Abstract

Microalgae have emerged as promising photosynthetic microorganisms for biofabricating advanced tissue constructs, with improved oxygenation and reduced reactive oxygen species (ROS) production. However, their use in the engineering of human tissues has been limited due to their intrinsic growth requirements, which are not compatible with human cells. In this study, we first formulated alginate–gelatin (AlgGel) hydrogels with increasing densities of *Chlorella vulgaris*. Then, we characterised their mechanical properties and pore size. Finally, we evaluated their effects on cardiac spheroid (CS) pathophysiological response under control and ischemia/reperfusion (I/R) conditions. Our results showed that the addition of *Chlorella* did not affect AlgGel mechanical properties, while the mean pore size significantly decreased by 35% in the presence of the 10^7 cells ml^{-1} microalgae density. Under normoxic conditions, the addition of 10^7 *Chlorella* cells ml^{-1} significantly reduced CS viability starting from 14 d in. No changes in pore size nor CS viability were measured for hydrogels containing 10^5 and 10^6 *Chlorella* cells ml^{-1}. In our I/R model, all *Chlorella*-enriched hydrogels reduced cardiac cell sensitivity to hypoxic conditions with a corresponding reduction in ROS production, as well as protected against I/R-induced reduction in cell viability. Altogether, our results support a promising use of *Chlorella*-enriched Alg–Gel hydrogels for cardiovascular tissue engineering.

1. Introduction

Microalgae have emerged as microorganisms that could be used in a wide range of biomedical applications, such as drug delivery systems, injectable hydrogels, and 3D bioprinted scaffolds [1–4]. Microalgae's intrinsic properties to produce oxygen and antioxidants while removing carbon dioxide make them promising candidates to prevent and treat oxygen deficiency-driven human diseases [5, 6].

However, these photosynthetic microorganisms require specific growth conditions (e.g., light exposure, nitrogen and phosphorus enriched media, pH and temperature), and they are very sensitive to contaminants, such as fungi and bacteria, whose relationship can be symbiotic or parasitic [7, 8]. Therefore,

the maintenance of strict aseptic conditions and minimising a potential phototoxic effect on mammalian cells, while avoiding excessive stress for microalgae, are the main challenges in addressing a cooperative environment between microalgae and human cells [2].

Among the wide variety of microalgae, *Chlorella vulgaris* is an unicellular green alga abundant in antioxidative, anti-inflammatory, hypolipidaemic and antihypertensive compounds, such as vitamin C, lutein, carotenoids, and tocopherol [9, 10]. Their antioxidative properties have been validated in both animal models and clinical trials, underlying *Chlorella vulgaris*' potential to effectively protect against oxidative stress in the body [9]. This sturdy strain also retains a great ability to adapt to a range of temperatures that are closer to the one present in the human body [11–13]. Despite several *in vitro* and *in vivo* studies have proven the microalgae protective role in cancer, wound healing, and hypoxic brain injuries, their potential roles in cardiovascular pathophysiology remain unexplored [14–18].

Cardiovascular disease including myocardial infarction (MI) represents a global cause of morbidity and mortality [19]. MI results from coronary arterial occlusion which leads to ischemic damage of the myocardial tissue [20]. The ischemic condition deprives the cardiac muscle of oxygen and nutrients, resulting in a cascade of molecular events that trigger mitochondrial dysfunction and reactive oxygen species (ROS) production [21]. As a result, injured cardiac cells lose their ability to balance ROS production, thus the accumulation of these toxic free radicals further exacerbates the cellular damage [21]. The reperfusion following ischemia is necessary to restore the blood flow to the myocardium [22]. However, this event leads to a burst in ROS generation, causing additional cellular injury, prolonged inflammation, and necrosis [22]. This complex scenario is known as ischemia/reperfusion (I/R) injury [21, 22]. Adverse sequelae of MI include compromised cardiac contractility, fibrotic restructuring, heightened susceptibility to arrhythmias, and systemic repercussions [22, 23]. One of the most severe consequences is heart failure, the chronic condition characterised by the heart's reduced ability to efficiently pump blood [24]. While the pivotal role of ROS during I/R injury in MI is well-established, the translation of these complex phenomena into *in vitro* models is very challenging, due to the intrinsic complexities of the *in vivo* human cardiac microenvironment, which is poorly recapitulated in small animal models [25].

Bioengineering of the cardiac microenvironment has offered advanced models to protect and treat cardiovascular disease, including personalised care [26–28]. In this regard, the development of advanced hydrogel formulations plays a pivotal role in the success of the biofabrication of viable and functional cardiac tissues, based on their tunable mechanical properties, ability to exchange oxygen and nutrients and effects on cell viability and function [29–32]. Among these, our team has bioengineered functional cardiac tissues as cardiac spheroids (CSs) that better mimic human cardiac pathophysiology compared to other existing models [33–35]. They mimic the complexity of the native cardiac tissue, creating a platform for advanced MI research [34, 36]. CSs have been used as *in vitro* models to elucidate disease mechanisms (i.e., I/R injury) and guide the development of novel cardioprotective strategies, with direct translation from the bench to the bedside [35–37]. We previously demonstrated that alginate–gelatin (AlgGel) hydrogels containing CSs are suitable to recapitulate the cardiac microenvironment mechanical properties, which positively promote cardiac cell viability and function *in vitro* and *in vivo* [35, 38, 39].

To date, other approaches have been taken to provide oxygen delivery and protection against ROS production in both I/R injury models and 3D bioengineered tissues, such as perfluorocarbon- [40, 41], haemoglobin-[42, 43], and peroxide-based carriers [44]. However, the risk of ROS overproduction, the limited oxygen-carrying capacity and the biocompatibility challenges represent the main drawbacks of these methods [45]. The use of photosynthetic microorganisms such as microalgae represents a valid alternative to other methods by providing a continuous, self-sustaining source of oxygen along with potent ROS scavenging capabilities, thereby addressing the dual need for oxygenation and oxidative stress reduction in I/R models [2]. In this study, we investigated for the first time if the addition of *Chlorella vulgaris* altered the mechanical properties of AlgGel hydrogels, as well as their potential to protect against oxidative stress-induced myocardial damage using our I/R *in vitro* model to investigate their effects on human CSs. Due to their antioxidant activity, we hypothesise that *Chlorella vulgaris* may prevent the increase in ROS production following I/R conditions and therefore protect against ROS-mediated myocardial damage *in vitro*. Here, first, we formulated hydrogels containing increasing densities of *Chlorella vulgaris*. And we characterised their mechanical properties and morphologies. Then, we embedded CSs in the *Chlorella*-enriched hydrogels to evaluate their effects on cell viability and ratio, as well as their potential protective role against myocardial injury *in vitro*. Alongside investigating the immediate protective effects of *Chlorella*-enriched hydrogels against I/R injury, we also aimed to evaluate the long-term biocompatibility and functional integration of CSs within these hydrogels. This approach is crucial for translating our findings from bench to bedside, ensuring that the *Chlorella*-enriched hydrogels not only provide acute protection but also support sustained cardiac function and tissue regeneration in potential clinical applications [39].

2. Experimental section

2.1. Materials

Alginic acid sodium salt from brown algae (low viscosity), Gelatin from bovine skin (Type B, powder, BioReagent, suitable for cell culture), calcium chloride ($CaCl_2$, anhydrous, powder, ⩾97%), Dulbecco's phosphate buffered saline (DPBS) with no calcium chloride nor magnesium chloride, agarose (BioReagent, for molecular biology), L-Glutamine solution (200 mM, sterile-filtered, BioXtra), Dulbecco′s Modified Eagle′s Medium (DMEM) high glucose, Triton™ X-100, bovine serum albumin (BSA, heat shock fraction, pH 5.2, ⩾96%) and formalin solution (neutral buffered, 10% 4% formaldehyde) were purchased from Sigma Aldrich (Castle Hill, NSW, Australia). Pen/Strep (Penicillin–Streptomycin (10000 U ml^{-1}, Gibco) was obtained from Thermo Fisher Scientific Australia (Scoresby, VIC, Australia). Purified mouse anti-human CD31 was purchased from BD Life Sciences, Macquarie Park, NSW, Australia). Secondary donkey anti-mouse antibody Alexa Fluor® 790-conjugated was purchased from Jackson ImmunoResearch Laboratories Inc. (West Grove, PA, United States). Troponin T-C Antibody (CT3) Alexa Fluor® 546-conjugated (cTNT) was obtained from Santa Cruz Biotechnology Inc. (Heidelberg, Germany). Alexa Fluor® 488 Anti-Vimentin antibody [V9] was purchased from Abcam (Melbourne, VIC, Australia). CellROX™ Green Reagent for oxidative stress detection, NucBlue™ Hoechst 33 342, Image-iT™ Red Hypoxia Reagent, and LIVE/DEAD™ Viability/Cytotoxicity Kit (calcein-AM and ethidium homodimer-1 (EthD-1)) were purchased from Thermo Fisher Scientific Australia (Scoresby, VIC, Australia).

2.2. Hydrogel preparation and crosslinking

Hydrogels were prepared according to our previously published protocols [35, 38]. Briefly, alginic sodium salt (Alg, 4% w/v) and gelatin (Gel, 8% w/v) powders were sterilised under UV light for 30 min. DMEM with 1% (v/v) Pen/Strep and 1% (v/v) L-glutamine 200 mM was heated at 50 °C and the Alg and Gel powders were slowly added until complete solubilisation under continuous stirring in sterile conditions. The AlgGel hydrogel was aliquoted, sealed, and then stored at 4 °C for further use. AlgGel hydrogels were enriched with increasing densities of microalgae (see section 2.5 for cell culture details) by slowly mixing the microalgae pellet in a warm (37 °C) AlgGel hydrogel until a homogeneous suspension was achieved. For the ionic crosslinking of AlgGel hydrogels, a sterile 2% w/v $CaCl_2$ solution was added on top of cold hydrogels [38].

2.3. Mechanical characterisation of hydrogels

The mechanical properties of the hydrogels were determined by both Brillouin microspectroscopy and rheology as per our previously published protocols [35] (figure 1(A)).

Briefly, the Brillouin microspectroscopy system consisted of a laser with approx. 200 mW continuous wave emission at 660 nm wavelength (Torus, Laser Quantum, Thebarton, SA, Australia), integrated with a confocal microscope (CM1, The Table Stable Ltd, Mettmenstetten, Switzerland), a 3D scanning microscopy stage (SmarAct, Oldenburg, Germany) and a 6-pass scanning tandem Fabry–Perot interferometer (The Table Stable Ltd, Mettmenstetten, Switzerland). This system was used to collect the spontaneous Brillouin scattering spectra, where the backscattered light was collected by an objective lens (20× Mitutoyo Plan Apo infinity corrected objective, NA = 0.42, WD = 20 mm) and subsequently redirected to the interferometer for analysis. The analysis was carried out on hydrogels before and after crosslinking and after incubation in DMEM (in the incubator at 37 °C, 5% CO_2) to avoid hydrogel dehydration. Each sample was analysed four times by recording the raw spectra of Stokes and Anti-Stokes Brillouin peaks at arbitrary points within each hydrogel sample. The collected raw data were analysed by fitting a Lorentzian model to every Stokes and Anti-Stokes Brillouin peak, produced as the result of optoacoustic interaction within the gel, using Ghost Software vers. 7.00 (The Table Stable Ltd, Mettmenstetten, Switzerland) to determine the average value and standard deviation of the Brillouin frequency shift (BFS, GHz) [46]. Results from the analyses of *Chlorella*-enriched hydrogels are reported as differences in BFS (ΔBFS) against AlgGel hydrogels.

In addition to Brillouin measurements, hydrogels were also analysed with a dynamic hybrid rheometer (TA Instruments, New Castle, DE, United States). The Young's moduli were calculated through unconfined compression. Each sample was moulded using 8 mm diameter disposable punch biopsies (KAI's Medical Products, Japan) and placed between the upper (8.0 mm parallel plate, Peltier plate Stainless steel, TA Instruments, New Castle, DE, United States) and lower geometries. The unconfined compression test was performed at 25 °C with a constant compression rate of 2 $\mu m\ s^{-1}$, by recording the axial force (N) and gap (μm) values as output data. The collected data were processed to obtain a stress versus strain curve for each replicate ($n = 4$), and Young's modulus (kPa) was calculated from the linear region. For the shear rheology measurements, an oscillatory amplitude sweep test was performed with a constant frequency of 0.159 Hz and strain amplitudes ranging from 0.2% to 2% within the linear viscoelastic region [35, 47].

2.4. Scanning electron microscopy and pore size analysis

The inner microstructure of Alg–Gel hydrogels with or without *Chlorella vulgaris* was assessed by scanning

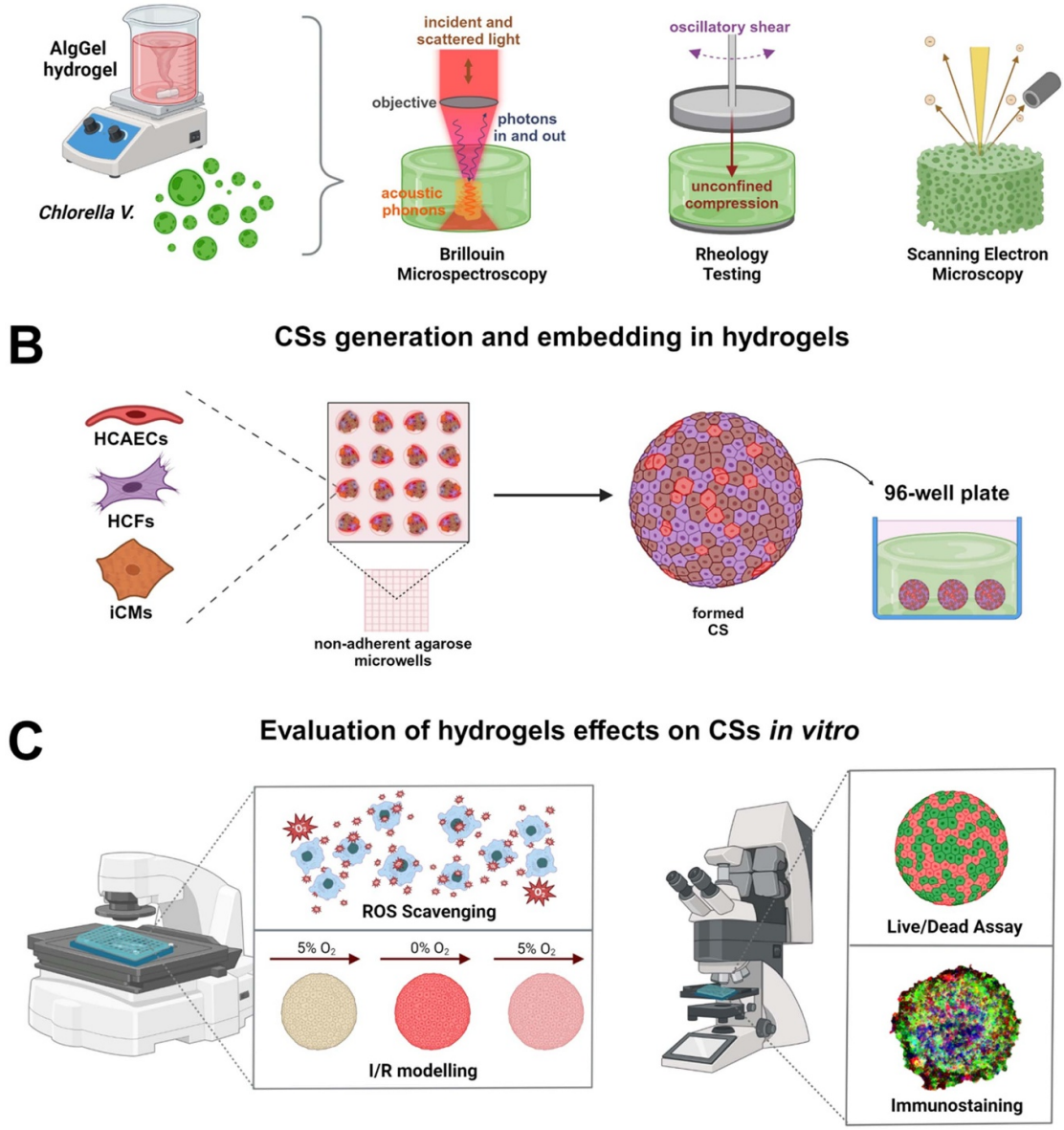

Figure 1. Schematic representation of the experimental plan. (A) Hydrogels enriched with *Chlorella vulgaris* cells were prepared in sterile conditions and fully characterised by Brillouin microspectroscopy, shear rheology, unconfined compression testing, and scanning electron microscopy. (B) HCAECs, HCFs, and iCMs were first cultured separately, then co-cultured in non-adherent agarose microwells, and incubated until compact CSs were formed. The CSs were plated in 96-well plates and embedded in Alg–Gel hydrogels. (C) CSs embedded in Alg–Gel hydrogels cultured in I/R and normoxic conditions before assessing the potential impact on cardiac cell viability, as well as their ROS scavenging activity. Finally, any effects of *Chlorella vulgaris* on cell ratio in CSs were determined by immunostaining analyses.

electron microscopy as previously published [35] (figure 1(A)). Briefly, each hydrogel was crosslinked, mounted on stubs covered with double adhesive carbon tabs and fully dried in a vacuum oven (100 kPa, Gallenkamp OVA031.XX1.5, Manchester, United Kingdom) or in a freeze-dryer (Alpha 2–4 LSCplus, Martin Christ, Osterode am Harz, Germany) for 24 h. Then, the samples were coated with gold (10 nm) using a sputter coater machine (Leica EM ACE600, Leica Microsystems Pty Ltd, Macquarie Park, NSW, Australia) and imaged using the Zeiss EVO LS15 scanning electron microscope (Zeiss, Macquarie Park, NSW, Australia), equipped with a thermionic tungsten electron gun, at 10 kV acceleration voltage of and 10.5 mm working distance. The same settings were used to image *Chlorella* cells alone, after fixing the pellet in 4% paraformaldehyde for 2 h, followed by a series of dehydration steps of increasing ethanol concentrations (10%–100%). Algae cells were then freeze-dried for 24 h before sputtering and imaging. Images of at least 12 random areas for each sample were acquired through the Zeiss SmartSEM operating system and analysed for pore size (area, μm^2) using ImageJ software [35, 48, 49].

2.5. Microalgae culture and quantum yield evaluation

Microalgae cells from the freshwater species *Chlorella vulgaris* (UTS-LD strain) were kindly provided by the Climate Change Cluster (University of Technology Sydney, Sydney, NSW, Australia). *Chlorella vulgaris* (or *Chlorella*) cells were cultured at 20 °C in MLA medium as previously reported [50]. In order to expand the number of *Chlorella*, an aliquot from the mother culture of *Chlorella* cells was collected and diluted in MLA medium (1:100 (v/v)). Then, cells were counted with a hemocytometer and finally centrifuged at 6000 rpm for 10 min at 20 °C to obtain a stable pellet [50].

To measure the photosynthetic activity of *Chlorella* cells we used an AquaPen-C AP 110-C device (Photon Systems Instruments, Drásov, Czech Republic). Different aliquots of *Chlorella* cells were cultured at either 20 °C or 37 °C and within a library of medium (containing either MLA or DMEM and a mix of the two) before evaluating their quantum yield as a measure of their photosystem II (PSII) efficiency.

2.6. Human cell cultures and CS generation

Human CSs were prepared as previously reported [33–35]. Briefly, human cardiac fibroblasts (HCFs) and human coronary artery endothelial cells (HCAECs) were obtained from Cell Applications (San Diego, CA, United States) and cultured in HCFs Medium and MesoEndo Growth Medium (Cell Applications, Inc, San Diego, CA, United States. iCell® Cardiomyocytes (iCMs) were obtained from FujiFilm Cellular Dynamics (Madison, WI, USA). iCMs were plated in iCell® Plating Medium for one day and then cultured in iCell® Maintenance Medium for 2 d (Fujifilm Cellular Dynamics, Inc., Madison, Wisconsin, USA) according to the manufacturer protocol.

Human CSs were prepared by co-culturing HCFs, HCAECs, and iCMs at a ratio of 1:1:2, respectively, in CS medium (HCF medium, MesoEndo growth medium, and iCell® maintenance medium at a 1:1:2 ratio) [35, 36]. The cell suspension was seeded in a non-adherent 2% (w/v) agarose 3D Petri Dishes®, pre-formed according to the manufacturer's instruction (Microtissues Inc., Providence RI, USA), and the constructs were incubated at 37 °C, 5% CO_2 (figure 1(B)). The CS medium was changed every 2 d until the CSs were formed. For *in vitro* studies and imaging the CSs ($n \geqslant 3$) were plated in bottom glass 96-well plates (Miltenyi Biotec, Macquarie Park, NSW, Australia) and a warm hydrogel (100 μl, 37 °C) was added on top. After gelation, the samples were crosslinked on ice and the CS medium was added on top before incubation. The samples were cultured at 37 °C, 5% CO_2 for up to 28 d, replacing the medium every 2 d (figure 1(C)) [34].

2.7. *In vitro* model of I/R damage and ROS scavenging activity evaluation in CSs

In order to model the I/R damage that human cardiac tissue experiences during MI, we used our previously established model using CSs [36]. Briefly, CSs were cultured at 37 °C with a range of oxygen concentrations to simulate normoxic conditions (5% O_2, 5% CO_2) for 24 h, followed by hypoxic conditions (0% O_2, 5% CO_2) for 24 h reproducing the ischemic event, and finally restoring the standard oxygenation (5% O_2, 5% CO_2) to mimic the reperfusion phase for further 24 h. Experiments were carried out by using a live imaging fluorescence microscope (EVOS M7000 Imaging System, Thermo Fisher Scientific Inc., Scoresby, VIC, Australia) equipped with an incubator stage (EVOS Onstage Incubator, Thermo Fisher Scientific Inc., Scoresby, VIC, Australia) for fine control of temperature, gases, and humidity. To track the intracellular oxygen concentration, a reversible fluorogenic reagent 10 μm Image-iT™ (Thermo Fisher Scientific Inc., Scoresby, VIC, Australia) was added to the medium. The CSs were imaged at the end of normoxia, hypoxia, and reperfusion [51]. Each hydrogel (with and/or without *Chlorella*) was considered an individual group, hence the fluorescence intensity values during induced hypoxia and reperfusion were normalised against the fluorescence derived from the normoxic condition.

To detect the oxidative stress level in CSs during I/R events, 5 μm CellROX™ Green Reagent (Thermo Fisher Scientific Inc., Scoresby, VIC, Australia) was added to the wells after the reperfusion step was completed. After 1 h of incubation at 37 °C, 5% CO_2, the samples were washed 3 times with PBS and imaged with EVOS M7000 Imaging System (Thermo Fisher Scientific Inc., Scoresby, VIC, Australia) [52, 53]. The collected images were processed in ImageJ to measure the fluorescence intensity of Image-iT™ and CellROX™ [49]. The data collected from the analysis of CellROX™ fluorescence of CSs after the I/R were normalised against the fluorescence of CSs cultured in normoxic conditions for three days.

2.8. Contractile activity and optical mapping measurements

To measure the contraction frequency (number of CS contractions per second) and the fractional shortening % (FS%), we recorded videos of contracting CSs using the EVOS M7000 Imaging System (Thermo Fisher Scientific Inc., Scoresby, VIC, Australia) after the I/R modelling, and after 3, 14 and 28 d of incubation in normoxic conditions (37 °C, 5% CO_2), as previously described [54].

To measure the conduction velocity (CV), CSs were plated in an 8-well chamber and incubated for 14 d at 37 °C, 5% CO_2. CS-containing wells were loaded with 17.7 μm Rhod-2 AM (fluorescent Ca^{2+} indicator, Abcam, Melbourne, VIC, Australia), 0.02% Pluronic™ F127 (Thermo Fisher Scientific Inc.,

Scoresby, VIC, Australia), and 50 μm RH237 (Santa Cruz Biotechnology Inc., Heidelberg, Germany) and incubated for 2 h at 37 °C, 5% CO_2. Each well was then washed with fresh culture medium three times and incubated for an additional 30 min with media prior to the individual transfer of CSs to 60 mm sterile cell culture plates (Corning). When ready for imaging, CSs were carefully moved to the OMS-PCIE-2002 optical mapping chamber (Mapping Lab Ltd, Manchester, UK) under an upright microscope equipped with high-speed CMOS cameras. Briefly, RH237 fluorescence as a function of the action potential was passed through a long-pass dichroic filter of 700 nm (FELH700, Thorlabs, Newton, NJ, USA), while Rhod-2 AM fluorescence as a function of Ca^{2+} was passed through a long-pass dichroic filter of 585 nm (FBH585, Thorlabs, Newton, NJ, USA). Both fluorescence signals were collected through a long pass dichroic beamsplitter with a cutoff wavelength of 638 nm (DMLP638, Thorlabs, Newton, NJ, USA), then filtered by a 550 nm long pass filter (FELH550, Thorlabs, Newton, NJ, USA) before voltage signals were imaged. A spatial resolution maximum of 512-by-512 pixels was utilized during acquisition, with a total mapping area of 64 × 64. Temporal resolution was set to 1000 frames/second at an exposure time of 0.9 ms over 10 s of recording time. Data was acquired in real-time using an 8-channel TTL analog-digital converter and OMapRecord 4.0 software (Mapping Lab Ltd, Manchester, UK), then processed using OMapScope 5.6.8 (Mapping Lab Ltd, Manchester, UK). Processing filters were applied to generate waveforms with low noise-to-signal ratios including a Gauss convolution of 9 × 9, a zero-phase filter window of 30, and theta smoothing intensity of 1.5. Waveform graphs were selected based on a selected region of interest to display the lowest signal-to-noise ratio. A single peak representing a single contraction was used for calculating the CV values for action potential and calcium signals, per array, including temporal sequence recordings (slowed to 1/20th of the original speed) to display the propagation of signals at different regions of the CSs.

2.9. Live/Dead staining and immunostaining of CSs

To evaluate any effects of *Chlorella*-enriched hydrogels on cell viability in embedded CSs, the dead/live cell ratios were measured up to 28 d, as previously described [35, 38]. Briefly, LIVE/DEAD™ Viability/Cytotoxicity Kit and NucBlue™ were used to detect living, dead and total cells by staining them with calcein-AM, EthD-1, and Hoechst, respectively. 1 μl ml^{-1} Calcein-AM, 1 μl ml^{-1} EthD-1 and Hoechst were directly added to the medium and CSs were incubated at 37 °C, 5% CO_2 for 3 h. After the incubation, the samples were washed 3 times with warm DPBS and imaged with a STELLARIS 8 CM1 (Leica Microsystems Pty Ltd, Macquarie Park, NSW, Australia). After the exposure to I/R, CSs were stained with calcein-AM and EthD-1 to evaluate the toxicity ratio. Control CSs were cultured under normoxic conditions and stained after three days. The autofluorescence of chlorophyll allowed the detection of surrounding *Chlorella* cells together with live and dead cells within the spheroids, both in normoxic conditions and after I/R. The data collected at each time point were presented as CS toxicity ratios (fluorescence of dead cells/fluorescence of live cells) and normalised against the toxicity ratio of CS embedded in AlgGel.

For immunostaining analyses, the samples were first fixed in 4% paraformaldehyde for 3 h at room temperature, washed in PBSA 0.01% (DPBS containing 0.01% sodium azide), permeabilised in 0.02% Triton-X/PBSA solution for 1 h, blocked with 3% BSA/PBSA solution, and then incubated with primary and secondary antibodies at 4 °C for 18 h [36]. HCAECs were labelled by using primary mouse anti-human CD31 (6.25 μg ml^{-1}) and secondary donkey anti-mouse Alexa Fluor® 790-conjugated antibody (21 μg ml^{-1}). CSs were also stained with Troponin T-C Antibody (CT3) Alexa Fluor® 546-conjugated (10 μg ml^{-1}), Alexa Fluor® 488 Anti-Vimentin antibodies (2 μg ml^{-1}) and NucBlue™ (2 drops ml^{-1}) to stain for iCMs, HCFs and nuclei, respectively. The collected images were processed in ImageJ and Adobe Photoshop 25.3.1 (Adobe Systems, In., San Jose, CA, USA) [49]. Each staining was measured individually and data were normalised against CSs embedded in AlgGel hydrogels.

2.10. Statistical analyses

All the collected data were analysed and plotted using GraphPad Prism version 8.4.2 for Windows (GraphPad Software, Boston, MA, USA). To evaluate the effect of *Chlorella*-enriched hydrogels on intracellular oxygen concentrations of CSs during the I/R *in vitro* modelling, ordinary two-way ANOVA followed by Tukey's multiple comparison tests were performed. To evaluate the contractile activity of CSs embedded in *Chlorella*-enriched hydrogels, ordinary one-way ANOVA followed by Dunnet's multiple comparisons tests were performed. For all the other analyses, Brown–Forsythe and Welch ANOVA followed by Dunnett's multiple comparisons tests were employed. All results are expressed as mean ± standard error mean (SEM).

3. Results

3.1. The presence of Chlorella cells does not affect the mechanical properties of AlgGel hydrogels

First, we prepared AlgGel hydrogels with increasing densities of *Chlorella*. We decided on three different numbers of *Chlorella* cells per AlgGel hydrogel based on previous studies including microalgae cell-containing hydrogels for biomedical applications [14, 55–57]. The composition (number of cells ml^{-1}) and

Table 1. Chlorella cells densities included in AlgGel to formulate Chlorella-enriched hydrogels.

Hydrogel abbreviation	Cells ml^{-1}
Chlo5	1×10^5
Chlo6	1×10^6
Chlo7	1×10^7

abbreviations of hydrogels prepared are summarised in table 1.

The autofluorescence at 680 nm of the chlorophyll contained within microalgae cells helped to detect the presence of *Chlorella* in AlgGel hydrogels after their crosslinking with $CaCl_2$ without the need for further staining using a 685/40 emission filter [58].

To evaluate any changes in the mechanical properties of previously characterised AlgGel hydrogel [35], these new hydrogels were studied as described below. Chlo5, Chlo6, and Chlo7 hydrogels were first tested with Brillouin microspectroscopy to study their viscoelastic properties (figures 2(A)–(C)). An AlgGel hydrogel without any *Chlorella* cells was prepared as a negative control. Brillouin microspectroscopy is a unique contactless and non-destructive technique that provides an understanding of local mechanical properties with microscopic spatial resolution by examining the interaction between light and high-frequency acoustic waves (or phonons) within a material [46, 59, 60]. The change in frequency of the scattered light due to the light-sound interaction is known as BFS (hereafter abbreviated as frequency shift), whose magnitude is directly related to the material's longitudinal elastic modulus [61, 62].

We analysed AlgGel and *Chlorella*-enriched hydrogels before crosslinking, after crosslinking, and after incubation with the cell medium. From the evaluation of the differences in BFS (ΔBFS), we did not measure any statistically significant changes ($p < 0.05$) between *Chlorella*-enriched hydrogels and AlgGel within each group (figures 2(A)–(C)). Taking into consideration that all samples were crosslinked and incubation with cell medium in the same way, these results indicate that the addition of *Chlorella* to AlgGel hydrogel does not affect its mechanical properties.

To confirm the mechanical behaviour of the hydrogels measured using Brillouin microscopy, we performed unconfined compression and oscillatory amplitude sweep testing (figures 2(D) and (E)). The Young's moduli of the hydrogels, calculated by extrapolation from the stress versus strain curves, confirmed the absence of statistically significant changes between AlgGel and *Chlorella*–enriched hydrogels (figure 2(D)). Indeed, figure 2(D) shows how *Chlorella*-enriched hydrogels elastically behaved similarly to AlgGel alone under the applied force. For Chlo7 we detected a Young's modulus after crosslinking of 24.4 ± 1 kPa compared to 23.7 ± 1.2 kPa of pure AlgGel. Taking into account that Young's modulus range of a diastolic adult human myocardium is in the range of 8–15 kPa and the tissue stiffening that takes place consequent to the early stages of MI, all the formulated hydrogels were considered suitable for further *in vitro* evaluations that include the embedding of CSs in hydrogels [63]. Furthermore, the oscillatory amplitude sweep test showed a complete overlapping of the curves related to both storage moduli (G') and loss moduli (G'') of all samples (figure 2(E)). A similar trend was measured in our Brillouin microspectroscopy analyses, indicating no statistically significant changes in the viscoelastic properties across samples.

3.2. Increasing concentrations of Chlorella cells in Alg/Gel hydrogels decreases their pore size

To identify any change in the hydrogel morphology, we performed scanning electron microscopy analyses to measure their pore size following the addition of increasing densities of *Chlorella* cells. Figure 3 indicates the representative scanning electron microscopy images along with the related analysis of the pore size of AlgGel and *Chlorella*-enriched hydrogels. Chlo5 hydrogel presents a pore size of 0.94 ± 0.82 μm, comparable to AlgGel's mean value of 0.96 ± 0.95. For Chlo6 and Chlo7 hydrogels, the porosity was found to be slightly smaller than in AlgGel hydrogels, with a size trend that was inversely proportional to the density of microalgae cells. Only Chlo7 had a significant reduction in pore size ($p < 0.001$), shrinking the pores by 35% when compared to AlgGel. Additional analyses of the pores by freeze-drying the samples (figure S2) before scanning electron microscopy imaging confirmed a ~50% reduction in pore size for Chlo7 compared to AlgGel hydrogels.

3.3. Chlorella–enriched hydrogels modulate oxygen sensitivity and improve the viability of CSs during I/R

To evaluate the effects of *Chlorella*-enriched hydrogels on cardiac cell sensitivity to oxygen deprivation, we employed our previously established *in vitro* model of I/R injury [36]. Our previous studies demonstrated that CSs finely recapitulate the cardiac microenvironment and they represent an advanced model to study I/R-driven myocardial damages [33, 36]. Image-iT™ was used to continuously track the intracellular oxygen concentration from the incubation in normoxic condition (5% O_2 and 5% CO_2), through the hypoxia (0% O_2 and 5% CO_2) and until the end of the reperfusion phase (5% O_2 and 5% CO_2) (figure S1) [51]. The lowest the intracellular oxygen concentration the highest the intensity of the Image-iT™ fluorescence. Similar to what was previously reported, when CSs in AlgGel hydrogels were exposed to 0% O_2 concentration, there was an increase in the fluorescence intensity of Image-iT™ (figure 4(A)). After restoring the physiological 5% O_2 concentration, there

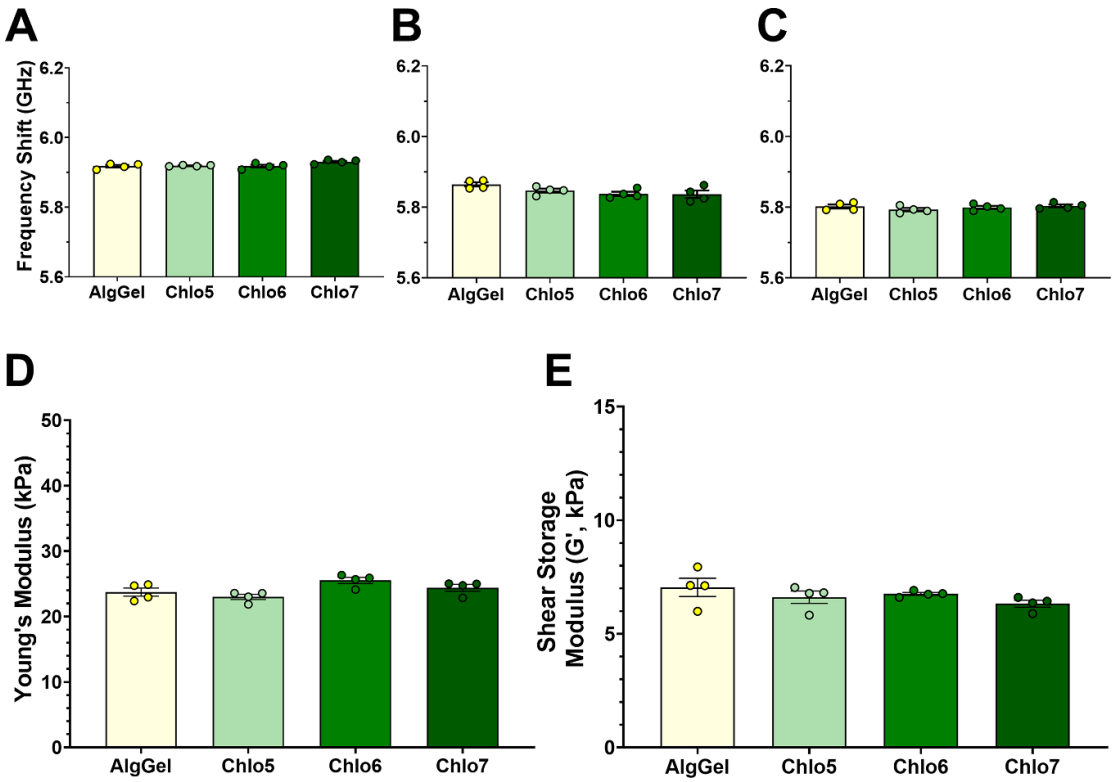

Figure 2. Brillouin microspectroscopy and rheology testing performed on AlgGel and *Chlorella*-enriched hydrogels. (A)–(C) Differences in Brillouin frequency shift (ΔBFS) between *Chlorella*-enriched and AlgGel hydrogels before cross-linking (A), after cross-linking (B), and after incubation with the medium (C). (D) Young's moduli derived from an unconfined compression test, and (E) shear storage (G') and loss (G'') moduli derived from an oscillatory amplitude sweep test, recorded after cross-linking. Brown–Forsythe and Welch ANOVA test was used to compare the groups. Error bars represent the mean $\pm$ SEM, if not visible they are within the symbols ($n = 4$).

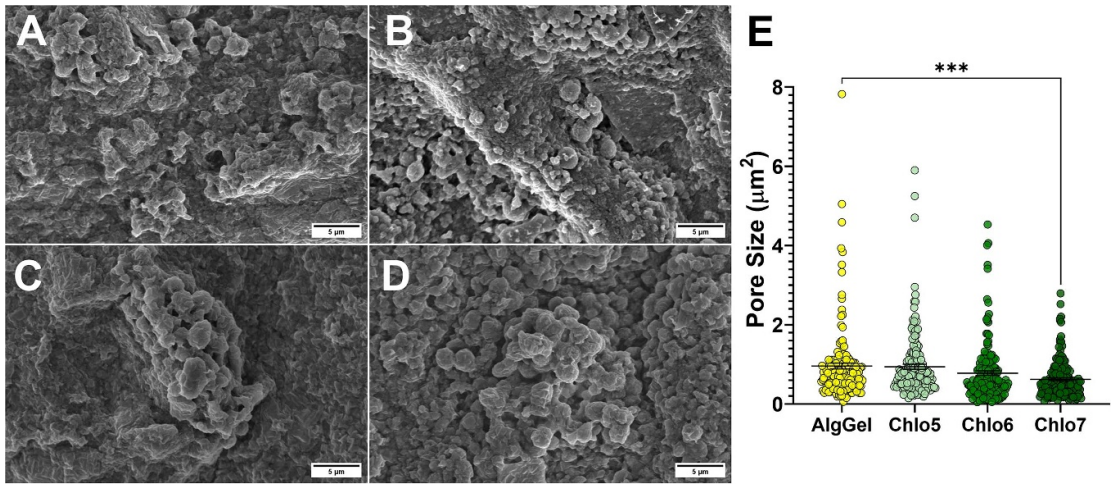

Figure 3. Scanning electron microscopy and pore size analyses of AlgGel and *Chlorella*-enriched hydrogels. Representative images from scanning electron microscope of (A) AlgGel, (B) Chlo5, (C) Chlo6, and (D) Chlo7. (E) Statistical analysis of pore size by using Brown–Forsythe and Welch ANOVA test to compare the groups (*** $p < 0.001$). Error bars represent the mean $\pm$ SEM, if not visible they are within the symbols ($n \geqslant 12$). Scale bars in images are equal to 5 μm.

was a decrease in fluorescence intensity (figure S1). However, the presence of microalgae led to a different outcome (figures 4(A)–(D)).

In fact, in the absence of extracellular O_2 (figure 4), microalgae significantly reduced intracellular hypoxia ($p < 0.0001$) among AlgGel and *Chlorella*-enriched hydrogels (figure 4(E)). The reduction of oxygen probe fluorescence positively correlated with the *Chlorella* cell density within the hydrogels. In particular, Chlo5, Chlo6 and Chlo7 hydrogels reduced the fluorescence intensity of Image-iT™ in CSs compared to CSs embedded in AlgGel alone, by 32%, 42%, and 54%, respectively.

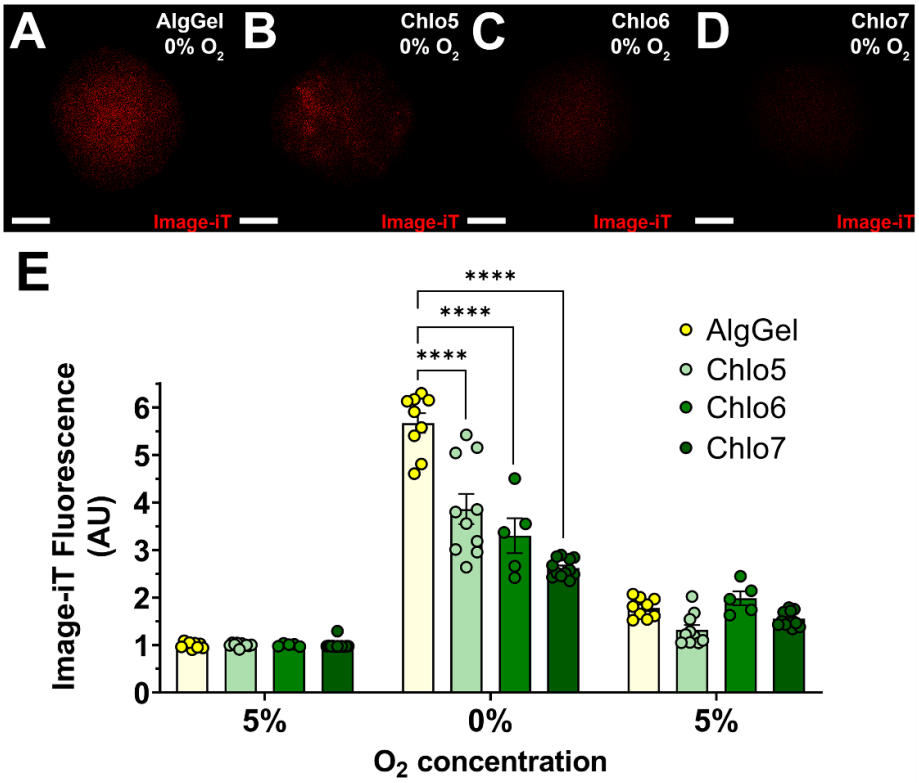

Figure 4. Intracellular O_2 concentration changes in CSs embedded in AlgGel and *Chlorella*-enriched hydrogels during I/R. Representative epifluorescent images of Image-iT™ during the hypoxia stage of I/R from CSs embedded in (A) AlgGel, (B) Chlo5, (C) Chlo6, and (D) Chlo7. (E) Statistical analysis of Image-iT™ fluorescence using ordinary two-way ANOVA followed by Tukey's multiple comparison tests to compare the groups (**** $p < 0.0001$). Error bars represent the mean ± SEM, if not visible they are within the symbols ($n \geqslant 5$). Scale bars in images are equal to 100 μm.

Our statistical analysis of CSs stained with dead and live dyes showed non-significant differences ($p > 0.05$) in toxicity ratio for Chlo5, Chlo6, and Chlo7 compared to CSs embedded in AlgGel after three days of incubation in normoxic conditions (figure 5(E)). On the contrary, a reduction in toxicity ratios was measured in CSs embedded in *Chlorella*-enriched hydrogels under I/R conditions (figure 5(J)). Compared to AlgGel, Chlo5, Chlo6, and Chlo7 reduced the toxicity ratio by 15%, 22%, and 29% ($p < 0.01$), respectively (figure 5(J)). To evaluate the long-term effects of *Chlorella*-enriched hydrogels on CS viability, we cultured them in normoxic conditions for up to 28 d. Figure S5 shows the representative confocal images of CSs stained with calcein-AM (live cells) and ethidium homodimer (dead cells) after 14 and 28 d in culture, respectively. After 14 d, CSs appeared still fully surrounded by *Chlorella* cells in Chlo5 and Chlo6 hydrogel, while in Chlo7 the microalgae cells seemed to migrate in the nearest proximity of CSs, leading to algae aggregates. Our statistical analyses (figure S5) show that CSs are viable in Chlo5 and Chlo6 hydrogels up to 28 d, whereas a significant ($p < 0.05$) increase in toxicity ratio was measured when they were cultured in Chlo7 already after 14 d.

3.4. Chlorella-enriched hydrogels protect against the reduction in contractile activity in I/R CSs

To evaluate the effects of *Chlorella*-enriched hydrogels on CS functionality, we measured the contraction frequency (Hz) and the FS% of CSs after 3 d of incubation in either normoxic conditions or after our I/R modelling. Chlo5 hydrogels were the only ones to significantly increase the contraction frequency ($p < 0.01$) in CSs cultured in normoxic conditions (figure 6(A)), whereas the addition of algae did not alter the FS% in CSs in normoxic conditions (figure 6(B)). On the contrary, the addition of algae improved the contractile function after I/R modelling. In fact, CSs embedded in Chlo5 and Chlo6 hydrogels exhibited a significant improvement in contraction frequency (figure 6(C)), while a significant increase in FS% was measured for all the tested hydrogels (figure 6(D)). The significant increase in contraction frequency ($p < 0.05$) observed for CSs embedded in Chlo6 was measured also at 14 d in

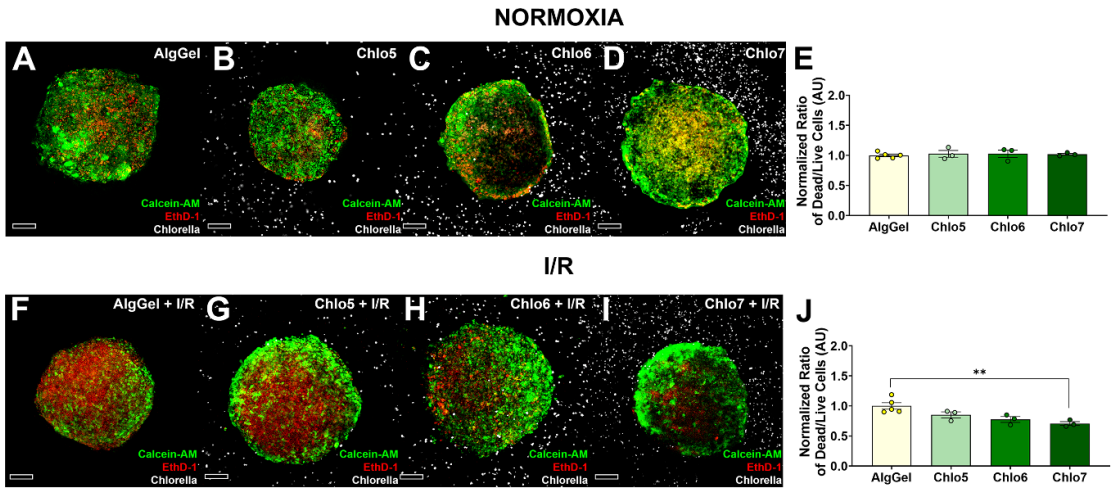

Figure 5. Toxicity ratios of CSs embedded in AlgGel and *Chlorella*-enriched hydrogels after incubation in normoxic and I/R conditions. Representative confocal images of Live/Dead assay of CSs embedded in hydrogels (A)–(D) incubated in normoxic conditions for three days and (F)–(I) after I/R injury. The images show the live (Calcein-AM) and dead (EthD-1) staining of CSs, additionally, *Chlorella* cells in hydrogel were visualised for their chlorophyll content. Statistical analysis of dead/live cells ratio in CSs (E) after 3 d of normoxic culturing conditions and (J) after I/R by using Brown–Forsythe and Welch ANOVA test to compare the groups (** $p < 0.01$). Error bars represent the mean ± SEM, if not visible they are within the symbols ($n \geqslant 3$). Scale bars in images are equal to 100 μm.

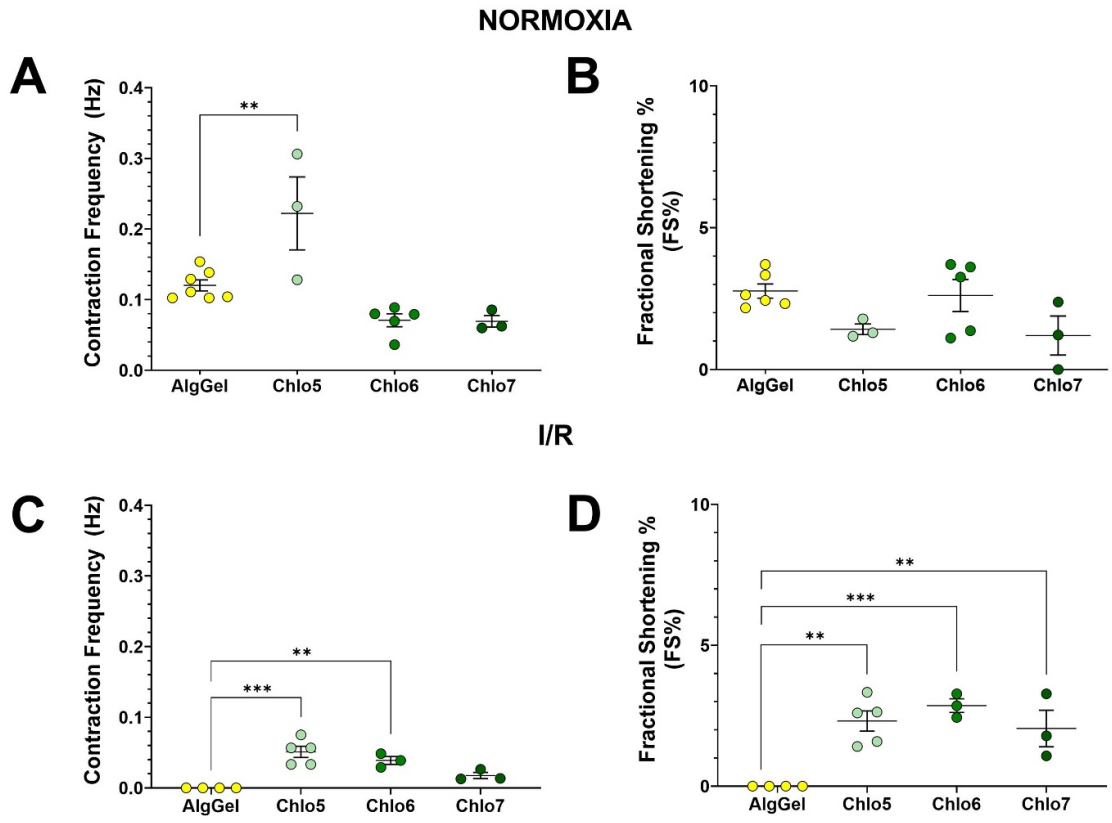

Figure 6. Contractile activity of CSs embedded in AlgGel and *Chlorella*-enriched hydrogels after incubation in normoxic and I/R conditions. Statistical analyses of contraction frequency (A), (C) and fractional shortening % (B), (D) of CSs using ordinary one-way ANOVA followed by Dunnett's multiple comparisons tests to compare the groups (** $p < 0.01$, *** $p < 0.001$). Error bars represent the mean ± SEM, if not visible they are within the symbols ($n \geqslant 3$).

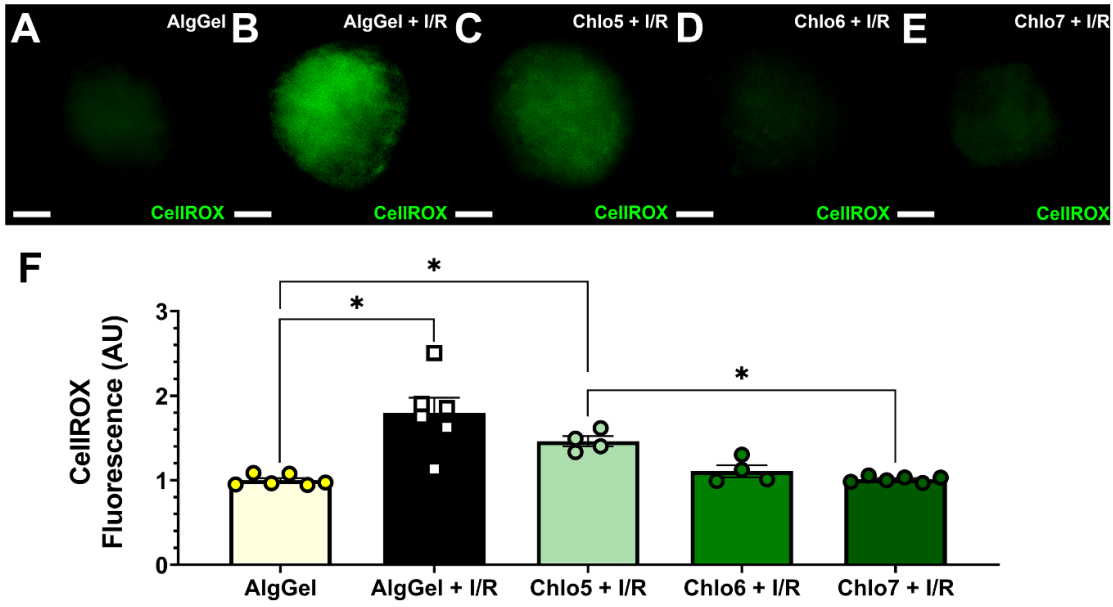

Figure 7. Intracellular ROS production changes in CSs embedded in AlgGel and *Chlorella*-enriched hydrogels after I/R. Representative epifluorescence images of CellROX™ fluorescence in CSs (A) embedded in AlgGel and cultured in normoxic conditions for 3 d, and after I/R embedded in (B) AlgGel, (C) Chlo5, (D) Chlo6, and (E) Chlo7. (F) Statistical analysis of CellROX™ fluorescence using Brown–Forsythe and Welch ANOVA test to compare the groups (* $p < 0.05$). Error bars represent the mean ± SEM, if not visible they are within the symbols ($n \geqslant 4$). Scale bars in images are equal to 100 μm.

normoxic conditions (figure S6) with no significant changes in the CV (figure S4).

3.5. Chlorella-enriched hydrogels exhibit ROS scavenging activity in I/R CSs

To evaluate *Chlorella*-enriched hydrogels' role in preventing ROS production, the CSs were incubated with CellROX™ to detect and quantify ROS generation immediately after I/R. We kept control CSs embedded in AlgGel in the incubator in normoxic conditions for the whole duration of the I/R experiment. The CSs used as control were incubated with CellROX™ simultaneously with I/R CSs, and finally imaged as shown in figures 7(A)–(E). The cell-permeant dye CellROX™ exhibits weak fluorescence in a reduced state, while it exhibits bright green fluorescence upon oxidation by ROS production. Our statistical analysis showed a significant increase ($p < 0.05$) in CellROX™ fluorescence for I/R CSs embedded in AlgGel compared to control normoxic CSs (figure 7(F)), confirming that ROS production increases during the I/R injury. Similarly, the increase in CellROX™ dye's fluorescence measured for CSs embedded in Chlo5 hydrogel was significant ($p < 0.05$) compared to the control normoxic CSs. On the contrary, CellROX™ fluorescence in Chlo6 and Chlo7 hydrogels was not significantly higher ($p > 0.05$) than control normoxic CSs, indicating that microalgae prevented an increase in ROS production during I/R injury.

3.6. The presence of Chlorella in hydrogels does not affect cardiac cell ratio in CSs

To evaluate if the presence of *Chlorella* cells in the AlgGel hydrogels could have affected cell populations within CSs, we imaged them after staining them with markers for cardiac endothelial cells, myocytes and fibroblasts after 28 d of incubation [33]. All cells were present either with or without microalgae (figure 8(A)). To assess if microalgae included in the hydrogel with different densities could have reduced or enhanced the cell distribution, we analysed the fluorescence obtained from each immunolabelling. Our statistical analysis of the cell presence in each CSs showed an increase in fibroblasts (Vimentin, green, figure 8(B)) as the microalgae density was increased. However, this increase was non-significant ($p > 0.05$) compared to CSs embedded in AlgGel alone. iCMs and HCAECs, labelled with cTNT and CD31, respectively, were not modified in their distribution by the surrounding *Chlorella* cells in the hydrogel.

4. Discussion

Here, we described for the first time a novel formulation of AlgGel hydrogels enriched with *Chlorella Vulgaris* for cardiac applications. As the presence of alginate used in hydrogels for cardiac applications might represent a limitation for cardiac cells' viability and function, it is generally used at a concentration of 1%–3% (w/v), alone or in combination with other polymers [64–67]. However, it has been shown that cardiac cells can adapt and grow while maintaining their function even at higher concentrations [68–70]. We previously demonstrated that CSs can live without any changes in their viability for up to 28 d when cultured in 4% Alg–8% Gel hydrogels [35]. More recently, we also showed that these hydrogels can be 3D bioprinted and transplanted in a mouse model of

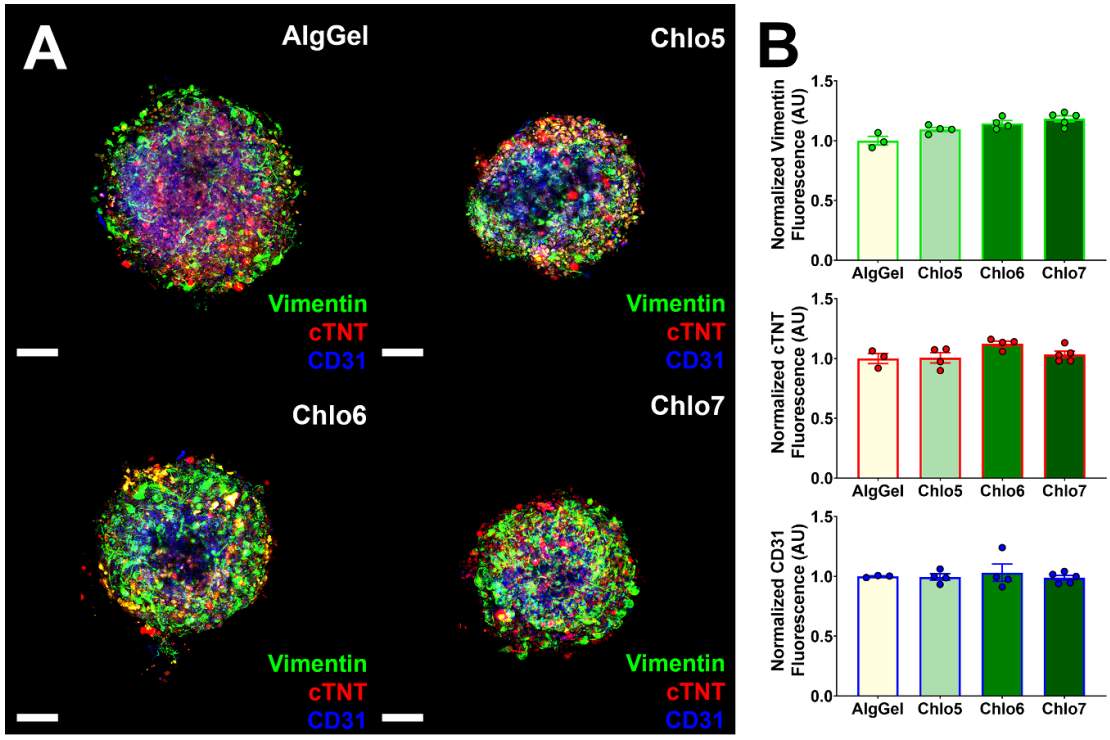

Figure 8. The addition of algae does not alter the presence of cardiac endothelial, myocytes and fibroblasts after 28 d in co-culture. Collapsed z-stacks of confocal images of representative CSs after 28 d of incubation with AlgGel and *Chlorella*-enriched hydrogel. (A) The CSs were stained with antibodies against Vimentin (green) for HCFs, cTNT (red) for iCMs, and CD31 (blue) for HCAECs. (B) Statistical analyses of stained cells fluorescence using Brown–Forsythe and Welch ANOVA test to compare the groups. Error bars represent the mean ± SEM, if not visible they are within the symbols ($n \geqslant 3$). Scale bars in images are equal to 100 μm.

MI for regenerative medicine purposes, ameliorating the cardiac function after a heart attack [39]. For this reason, in this study we only compared the addition of algae cells to 4%Alg–8%Gel hydrogels. We compared four distinct formulations with increasing *Chlorella* densities since the presence of microalgae in hydrogels could alter the viability of the cardiac human cells [4]. Our mechanical analyses showed that the addition of *Chlorella* cells did not alter either Young's moduli or the shear storage and loss moduli of AlgGel hydrogels (figures 2(D) and (E)), which have been previously demonstrated suitable for human cardiac tissue [35]. Young's moduli measured for all hydrogel formulations (figure 2(D)) demonstrated a greater stiffness and resistance to deformation than many inherently softer and more deformable hydrogels intended for biomedical applications (with Young's modulus ∼0.01–10 kPa) [71]. Brillouin microspectroscopy is a more sensitive technique than rheology, which allows to finely assess the viscoelastic properties of hydrogels by a non-invasive microscopic laser-based analysis at the microscopic level in 3D [59]. Our rheological measurements were consistent with Brillouin microspectroscopy analyses since no statistically significant changes in the BFS were recorded with the inclusion of increasing densities of *Chlorella* (figures 2(A)–(C)). This might suggest a homogenous inclusion of microalgae during the hydrogel formulation with an effective immobilisation of microalgae cells within the hydrogel polymeric network. Previous studies demonstrated the importance of a successful immobilisation of microalgae, which is crucial both to confine them within the hydrogel matrix and to control their growth and bioactive compound production [57, 72]. However, future studies might include Brillouin microspectroscopy analyses of *Chlorella*-enriched hydrogels incubated for 14 and 28 d to identify any potential long term effects of algae on hydrogel viscoelastic properties (figures 2(A)–(C)).

Together with their mechanical properties, the morphology of biomaterials plays an important role in controlling cell survival and function [73]. The more porous the material the greater the diffusion of nutrients, oxygen, and functional biomolecules across the network and the more favourable the removal of exhausted metabolic products and toxins from the cells [73]. Pore size and distribution also influence the facilitation of cell behaviours, such as adhesion, differentiation, and proliferation [74, 75]. Several studies demonstrated that highly porous scaffolds had positive effects on cardiac cell adhesion, viability and functionality under normoxic and disease conditions *in vitro* and cardiac function in animal models of MI *in vivo* [68, 74, 76–78]. Previous reports also demonstrated that the

reduction of pore size in CS-embedding hydrogels caused a significant decrease in cardiac cell viability [54]. On the other hand, with the increase of porosity, the hydrogel's ability to withstand mechanical stress may be weakened, resulting in more fragile and fast-degradable constructs that poorly mimic the ECM milieu [79]. Given *Chlorella*'s spherical shape and averaging size between 1–10 μm (figure S2), the addition of these microalgae within the polymeric network of AlgGel hydrogels could have implications for the flux of nutrients to the embedded CSs and limit the viability and functionality of cardiac cells [80]. *Chlorella*-enriched hydrogels which contained 10^5 and 10^6 cells ml^{-1} did not affect the mean pore size of AlgGel hydrogels, while the highest density (10^7 cells ml^{-1}) significantly reduced pore area (figures 3(E) and S2). The reduction in pore size could be related to higher production in microalgae biomass (i.e. proteins and polysaccharides) proportional to the microalgae density [81]. In this context, a previous study demonstrated that high production of proteins and polysaccharides from microalgae can interfere with the hydrogel's network formation and stability [81, 82]. However, considering that the mechanical analyses demonstrated that the incorporation of 10^7 *Chlorella* cells ml^{-1} did not affect the hydrogel's mechanical properties (figure 2), an alternative explanation for the reduction in pore size could be a physical occlusion of the pores by microalgae cells, rather than to the production of *Chlorella* biomass.

After generating human CSs *in vitro*, we embedded them in AlgGel hydrogels (with or without *Chlorella*) to evaluate microalgae effects on cardiac cells during normoxic conditions. Our toxicity ratio measurements after 3, 14, and 28 d of culture in normoxic conditions (figures 5 and S5) show that CSs were able to survive surrounded by Chlo5 and Chlo6 up to 28 d, without significant increases in toxicity ratio compared to AlgGel. However, we measured a significant increase in toxicity ratio after 14 d of culture Chlo7 hydrogels. This is consistent with the concentration-dependent cytotoxicity of *Chlorella* extracts previously demonstrated on different mammalian cell lines [83] and it is consistent with the reduction of pore size for Chlo7 measured based on our scanning electron microscopy analyses (figures 3(E) and S2). The reduction in pore size may have negatively affected the transport of nutrients for CSs to survive in the 3D microenvironment, as previously reported [54].

The pathophysiological events that occur during MI are closely related to the ischemic condition experienced by the myocardium. The sudden loss of blood supply to the cardiac tissue causes hypoxia, which leads to a depletion of intracellular ATP reserve, the shift to anaerobic metabolism, acidosis, and the following disruption of cellular osmotic balance, cellular oedema, and release of several inflammatory mediators [23, 84]. In addition, the reperfusion of myocardium leads to ROS production which nourishes the inflammatory and cell death pathways, exacerbating the cardiac cell injury [84, 85]. Therefore, we evaluated *Chlorella*-enriched hydrogels' protective role against myocardial damage in an *in vitro* model of I/R for the first time. Our toxicity ratio measurements proportionally increased with the addition of *Chlorella* cells after IR (figure 5(J)). During normoxic conditions, all CSs embedded in Chlo5, Chlo6, and Chlo7 increased the intracellular oxygen concentration as expected (measured as a reduction of the oxygen-sensitive dye used, figure 4). Moreover, while the contractile activity of CSs embedded in AlgGel hydrogel was abolished, the inclusion within *Chlorella*-enriched hydrogels offered protection from I/R to CSs by significantly increasing their contraction frequency and FS% (figures 6(C) and (D)). In the presence of *Chlorella* cells, the expected reduction in oxygen was prevented, supporting their role in modulating cardiac cells' sensitivity to hypoxia. This could be due to the oxygen dissolved from microalgae within the porous hydrogel structure [86, 87]. However, when we exposed *Chlorella* cells to new temperatures and medium compositions, we found that their quantum yield values were significantly reduced (figure S3). Quantum yield is a measure of the microorganisms' PSII efficiency and photosynthetic activity. The reduced photosynthetic activity could be due to suboptimal growing conditions or environmental stress [88, 89]. However, this would not impact the scaveging activity typical of algae. In fact, by assessing ROS scavenging activity, the higher the presence of *Chlorella* in hydrogels the lowest the ROS production from cardiac cells during the I/R (figure 7(F)). These results effectively support the promising protective role played by *Chlorella*-enriched hydrogels in modulating the I/R-driven myocardial damages *in vitro,* possibly due to either their scavenging or antioxidative properties, rather than an active oxygen production. Recently, *Chlorella* has gained a GRAS certification issued by the FDA for its consumption as a dietary supplement, thanks to its high-value composition rich in polyunsaturated fatty acids, phenolic compounds, carotenoids, vitamins C and E [10, 90, 91]. These bioactive compounds could have been the main players in exhibiting *Chlorella*-enriched hydrogels' protective role in CSs. Our immunolabelling in CSs for the three cardiac cell types (myocytes, endothelial cells and fibroblasts) demonstrated that the addition of *Chlorella* cells to AlgGel did not affect their presence (figure 8), which was comparable with the one of CSs embedded in AlgGel alone. Given their unique properties, future studies could aim to 3D bioprint *Chlorella*-enriched hydrogels as cardiac patches to be tested in an *in vivo* model of MI. Moreover,

it is critical to further validate whether *Chlorella*-enriched hydrogels can rescue changes that underpin mechanobiological mechanisms relevant to cardiovascular pathophysiology. This will pave the way for a more comprehensive understanding of the role played by *Chlorella*-enriched hydrogels to protect from MI injury.

5. Conclusion

In this study, we demonstrated for the first time that *Chlorella*-enriched hydrogels maintained the mechanical and structural properties of AlgGel hydrogels within a certain range of microalgae densities (10^5–10^6 cells ml^{-1}), without negatively affecting the cardiac cell viability for up to 28 d of co-culture. These results described the good compatibility of the *Chlorella* strain with human cardiac cells environment and growing conditions. The effects played by *Chlorella vulgaris* on hydrogel properties and cardiac cell viability were mostly dependent on the microalgae density incorporated within the polymeric network. Cho6 (10^6 *Chlorella* cells ml^{-1}) significantly reduces cardiac cell sensitivity to hypoxic conditions while it exhibits a consistent reduction in ROS production, without affecting either the mechanical properties or the pore size compared to the AlgGel hydrogel. Also, Chlo6 allows the culture of CSs for up to 28 d, without impacting the long-term viability of human cardiac cells and maintaining the same cellular presence. More interestingly, *Chlorella*-enriched hydrogels are useful to protect against I/R myocardial damage by providing ROS scavenging activity in bioengineered cardiac tissue. Altogether, our findings support the use of *Chlorella*-enriched hydrogels as advanced biomaterials for cardiac applications. We believe these systems have the potential to be used as model for facilitating the translation of 3D bioprinted cardiac patches made of microalgae-based hydrogels from bench to bedside, in addition to providing a novel therapeutic option for mitigating I/R injury through enhanced ROS scavenging activity.

Data availability statement

The data that support the findings of this study are openly available at the following URL/DOI: https://osf.io/pyru7/.

Acknowledgments

The authors would like to thank Louise Cole and Amy Bottomley for their technical assistance. In particular, we acknowledge the use of the Leica STELLARIS 8 confocal microscope in the Microbial Imaging Facility (MIF) in the Faculty of Science, the University of Technology Sydney. The authors are grateful to Herbert Yuan, Professional Officer in the Microstructural Analysis Unit (MAU) in the Faculty of Science, the University of Technology Sydney, who provided training and assistance for scanning electron microscopy imaging. Finally, we would like to thank Dr Yatong Li (MappingLab Ltd) for her kind assistance with optical mapping and conduction velocity measurements.

Financial support

Carmine Gentile was supported by a UTS Seed Funding, a UTS Cross-Faculty Grant, Heart Research Australia Grant, Perpetual IMPACT Grant, Catholic Archdiocese of Sydney Grant for Adult Stem Cell Research, and a Heart Research Institute Grant. Irina Kabakova and Hadi Mahmodi are supported by the Australian Research Council Centre of Excellence in Optical Microcombs for Breakthrough Science (CE230100006) and the Australian Research Council Centre of Excellence in Quantum Biotechnology (CE230100021). Thomas R Cox is supported by the National Health and Medical Research Council (NHMRC). Kaitlin Wyllie is supported by the University Postgraduate Award (UPA) from the University of New South Wales (UNSW). Donatella Paolino was supported by grants from the Italian Ministry of Health (PSC SALUTE 2014-2020-POS4 'Cal-Hub-Ria'-T4-AN-09 and PNRR MAD-2022-12376814).

ORCID iDs

Martine Tarsitano https://orcid.org/0000-0003-2331-7775
Clara Liu Chung Ming https://orcid.org/0000-0001-9414-3499
Hadi Mahmodi https://orcid.org/0000-0003-4820-5614
Kaitlin Wyllie https://orcid.org/0009-0008-5326-9894
Dana Idais https://orcid.org/0009-0006-8809-3505
Donatella Paolino https://orcid.org/0000-0002-5223-9879
Thomas R Cox https://orcid.org/0000-0001-9294-1745
Irina Kabakova https://orcid.org/0000-0002-6831-9478
Peter Ralph https://orcid.org/0000-0002-3103-7346
Carmine Gentile https://orcid.org/0000-0002-3689-4275

References

[1] Huang H, Lang Y, Wang S and Zhou M 2024 Microalgae-based drug delivery systems in biomedical applications *Eng. Regen.* **5** 361–74
[2] Ortega J S, Corrales-Orovio R, Ralph P, Egaña J T and Gentile C 2023 Photosynthetic microorganisms for the oxygenation of advanced 3D bioprinted tissues *Acta Biomater.* **165** 180–96

[3] Severo I A, Dias R R, Do Nascimento T C, Deprá M C, Maroneze M M, Zepka L Q and Jacob-Lopes E 2022 Microalgae-derived polysaccharides: potential building blocks for biomedical applications *World J. Microbiol. Biotechnol.* **38** 150
[4] Zhang Z, Chen Y, Klausen L H, Skaanvik S A, Wang D, Chen J and Dong M 2023 The rational design and development of microalgae-based biohybrid materials for biomedical applications *Engineering* **24** 102–13
[5] Cui H, Su Y, Wei W, Xu F, Gao J and Zhang W 2022 How microalgae is effective in oxygen deficiency aggravated diseases? A comprehensive review of literature *Int. J. Nanomed.* **17** 3101–22
[6] Eze C N, Onyejiaka C K, Ihim S A, Ayoka T O, Aduba C C, Ndukwe J K, Nwaiwu O and Onyeaka H 2023 Bioactive compounds by microalgae and potentials for the management of some human disease conditions *AIMS Microbiol.* **9** 55–74
[7] Laezza C, Salbitani G and Carfagna S 2022 Fungal contamination in microalgal cultivation: biological and biotechnological aspects of fungi-microalgae interaction *J. Fungi* **8** 1099
[8] Dolganyuk V, Belova D, Babich O, Prosekov A, Ivanova S, Katserov D, Patyukov N and Sukhikh S 2020 Microalgae: a promising source of valuable bioproducts *Biomolecules* **10** 1153
[9] Barghchi H *et al* 2023 The effects of Chlorella vulgaris on cardiovascular risk factors: a comprehensive review on putative molecular mechanisms *Biomed. Pharmacother.* **162** 114624
[10] Widyaningrum D and Prianto A D 2021 Chlorella as a source of functional food ingredients: short review *IOP Conf. Ser.: Earth Environ. Sci.* **794** 012148
[11] Krimech A, Helamieh M, Wulf M, Krohn I, Riebesell U, Cherifi O, Mandi L and Kerner M 2022 Differences in adaptation to light and temperature extremes of Chlorella sorokiniana strains isolated from a wastewater lagoon *Bioresour. Technol.* **350** 126931
[12] Coronado-Reyes J A, Salazar-Torres J A, Juarez-Campos B and Gonzalez-Hernandez J C 2020 Chlorella vulgaris, a microalgae important to be used in biotechnology: a review *Food Sci. Technol.* **42** e37320
[13] Ru I T K, Sung Y Y, Jusoh M, Wahid M E A and Nagappan T 2020 Chlorella vulgaris: a perspective on its potential for combining high biomass with high value bioproducts *Appl. Phycol.* **1** 2–11
[14] Cohen J E *et al* 2017 An innovative biologic system for photon-powered myocardium in the ischemic heart *Sci. Adv.* **3** e1603078
[15] Corrales-Orovio R, Carvajal F, Holmes C, Miranda M, González-Itier S, Cárdenas C, Vera C, Schenck T L and Egaña J T 2023 Development of a photosynthetic hydrogel as potential wound dressing for the local delivery of oxygen and bioactive molecules *Acta Biomater.* **155** 154–66
[16] Obaíd M L *et al* 2021 A first in human trial implanting microalgae shows safety of photosynthetic therapy for the effective treatment of full thickness skin wounds *Front. Med.* **8** 772324
[17] Holmes C, Varas J, San Martín S and Egaña J T 2022 Towards an *in vitro* 3D model for photosynthetic cancer treatment: a study of microalgae and tumor cell interactions *Int. J. Mol. Sci.* **23** 13550
[18] Voss L J, Plouviez M and Whittle N 2021 Microalgae-based photosynthetic strategy for oxygenating avascularised mouse brain tissue-an *in vitro* proof of concept study *Brain Res.* **1768** 147585
[19] Tsao C W *et al* 2023 Heart disease and stroke statistics-2023 update: a report from the American heart association *Circulation* **147** e93–e621
[20] Del Buono M G, Moroni F, Montone R A, Azzalini L, Sanna T and Abbate A 2022 Ischemic cardiomyopathy and heart failure after acute myocardial infarction *Curr. Cardiol. Rep.* **24** 1505–15
[21] Bugger H and Pfeil K 2020 Mitochondrial ROS in myocardial ischemia reperfusion and remodeling. *Biochim. Biophys. Acta* **1866** 165768
[22] Liu Y, Li L, Wang Z, Zhang J and Zhou Z 2023 Myocardial ischemia-reperfusion injury; molecular mechanisms and prevention *Microvasc. Res.* **149** 104565
[23] Frantz S, Hundertmark M J, Schulz-Menger J, Bengel F M and Bauersachs J 2022 Left ventricular remodelling post-myocardial infarction: pathophysiology, imaging, and novel therapies *Eur. Heart J.* **43** 2549–61
[24] Schwinger R H G 2021 Pathophysiology of heart failure *Cardiovasc. Diagn. Ther.* **11** 263–76
[25] Rahman A, Li Y, Chan T K, Zhao H, Xiang Y, Chang X, Zhou H, Xu D and Ong S B 2023 Large animal models of cardiac ischemia-reperfusion injury: where are we now? *Zool. Res.* **44** 591–603
[26] Min S and Cho S W 2023 Engineered human cardiac tissues for modeling heart diseases *BMB Rep.* **56** 32–42
[27] Tang X Y, Wu S, Wang D, Chu C, Hong Y, Tao M, Hu H, Xu M, Guo X and Liu Y 2022 Human organoids in basic research and clinical applications *Signal Transduct. Target. Ther.* **7** 168
[28] Matthews N, Pandolfo B, Moses D and Gentile C 2022 Taking it personally: 3D bioprinting a patient-specific cardiac patch for the treatment of heart failure *Bioengineering* **9** 93
[29] Wu C A, Zhu Y and Woo Y J 2023 Advances in 3D bioprinting: techniques, applications, and future directions for cardiac tissue engineering *Bioengineering* **10** 842
[30] Elkhoury K, Morsink M, Sanchez-Gonzalez L, Kahn C, Tamayol A and Arab-Tehrany E 2021 Biofabrication of natural hydrogels for cardiac, neural, and bone tissue engineering applications *Bioact. Mater.* **6** 3904–23
[31] Li P, Hu J, Wang J, Zhang J, Wang L and Zhang C 2023 The role of hydrogel in cardiac repair and regeneration for myocardial infarction: recent advances and future perspectives *Bioengineering* **10** 165
[32] Montero P, Flandes-Iparraguirre M, Musquiz S, Pérez Araluce M, Plano D, Sanmartín C, Orive G, Gavira J J, Prosper F and Mazo M M 2020 Cells, materials, and fabrication processes for cardiac tissue engineering *Front. Bioeng. Biotechnol.* **8** 955
[33] Polonchuk L, Chabria M, Badi L, Hoflack J-C, Figtree G, Davies M J and Gentile C 2017 Cardiac spheroids as promising *in vitro* models to study the human heart microenvironment *Sci. Rep.* **7** 7005
[34] Sharma P and Gentile C 2021 Cardiac spheroids as *in vitro* bioengineered heart tissues to study. Human heart pathophysiology *J. Vis. Exp.* **167** 33554972
[35] Polonchuk L *et al* 2021 Towards engineering heart tissues from bioprinted cardiac spheroids *Biofabrication* **13** 34265755
[36] Sharma P, Liu Chung Ming C, Wang X, Bienvenu L A, Beck D, Figtree G, Boyle A and Gentile C 2022 Biofabrication of advanced *in vitro* 3D models to study ischaemic and doxorubicin-induced myocardial damage *Biofabrication* **14** 109–16
[37] Liu Y *et al* 2022 hESCs-derived early vascular cell spheroids for cardiac tissue vascular engineering and myocardial infarction treatment *Adv. Sci.* **9** e2104299
[38] Roche C D, Sharma P, Ashton A W, Jackson C, Xue M and Gentile C 2021 Printability, durability, contractility and vascular network formation in 3D bioprinted cardiac endothelial cells using alginate-gelatin hydrogels *Front. Bioeng. Biotechnol.* **9** 636257
[39] Roche C D, Lin H, Huang Y, de Bock C E, Beck D, Xue M and Gentile C 2023 3D bioprinted alginate-gelatin hydrogel patches containing cardiac spheroids recover heart function in a mouse model of myocardial infarction *Bioprinting* **30** e00263
[40] Radisic M, Park H, Chen F, Salazar-Lazzaro J E, Wang Y, Dennis R, Langer R, Freed L E and Vunjak-Novakovic G 2006

Biomimetic approach to cardiac tissue engineering: oxygen carriers and channeled scaffolds *Tissue Eng.* **12** 2077–91
[41] Jakovljevic V *et al* 2022 Dose-dependent effects of perfluorocarbon-based blood substitute on cardiac function in myocardial ischemia-reperfusion injury *Mol. Cell Biochem.* **477** 2773–86
[42] Faggiano S, Ronda L, Bruno S, Abbruzzetti S, Viappiani C, Bettati S and Mozzarelli A 2022 From hemoglobin allostery to hemoglobin-based oxygen carriers *Mol. Aspects Med.* **84** 101050
[43] Centis V, Proulx P and Vermette P 2011 PEGylated liposomes encapsulating human hemoglobin enhance oxygen transfer and cell proliferation while decreasing cell hypoxia in fibrin *Biochem. Eng. J.* **55** 162–8
[44] Fan Z, Xu Z, Niu H, Gao N, Guan Y, Li C, Dang Y, Cui X, Liu X L and Duan Y 2018 An injectable oxygen release system to augment cell survival and promote cardiac repair following myocardial infarction *Sci. Rep.* **8** 1371
[45] Jenabi A, Mehdinavaz Aghdam R, Ebrahimi S S, Ahmadi Tafti S H, Krishnan S, Suresh K S and Ramalingam M 2022 Oxygen delivery approaches to augment cell survival after myocardial infarction: progress and challenges *Cardiovasc. Toxicol.* **22** 207–24
[46] Mahmodi H, Piloni A, Utama R H and Kabakova I 2021 Mechanical mapping of bioprinted hydrogel models by Brillouin microscopy *Bioprinting* **23** e00151
[47] Rad M A, Mahmodi H, Filipe E C, Cox T R, Kabakova I and Tipper J L 2022 Micromechanical characterisation of 3D bioprinted neural cell models using Brillouin microspectroscopy *Bioprinting* **25** e00179
[48] Baptista M *et al* 2020 Silk fibroin photo-lyogels containing microchannels as a biomaterial platform for in situ tissue engineering *Biomater. Sci.* **8** 7093–105
[49] Schneider C A, Rasband W S and Eliceiri K W 2012 NIH image to ImageJ: 25 years of image analysis *Nat. Methods* **9** 671–5
[50] Bates H, Zavafer A, Szabó M and Ralph P J 2023 The slow-phase of chlorophyll fluorescence induction curve reflects the electron transport rates of photosystem II in vivo in Chlorella vulgaris *J. Appl. Phycol.* **35** 109–16
[51] Sharma P, Beck D, Murtha L A, Figtree G, Boyle A and Gentile C 2022 Fibulin-3 deficiency protects against myocardial injury following ischaemia/ reperfusion in *in vitro* cardiac spheroids *Front. Cardiovasc. Med.* **9** 913156
[52] Balkrishna A, Gohel V, Kumari P, Manik M, Bhattacharya K, Dev R and Varshney A 2022 Livogrit prevents methionine-cystine deficiency induced nonalcoholic steatohepatitis by modulation of steatosis and oxidative stress in human hepatocyte-derived spheroid and in primary rat hepatocytes *Bioengineered* **13** 10811–26
[53] Eguchi H, Kimura R, Onuma S, Ito A, Yu Y, Yoshino Y, Matsunaga T, Endo S and Ikari A 2022 Elevation of anticancer drug toxicity by caffeine in spheroid model of human lung adenocarcinoma A549 cells mediated by reduction in claudin-2 and Nrf2 expression *Int. J. Mol. Sci.* **23** 15447
[54] Vettori L *et al* 2024 Silk fibroin increases the elasticity of alginate-gelatin hydrogels and regulates cardiac cell contractile function in cardiac bioinks *Biofabrication* **16** 035025
[55] Wang X, Yang C, Yu Y and Zhao Y 2022 *In situ* 3D bioprinting living photosynthetic scaffolds for autotrophic wound healing *Research* **2022** 9794745
[56] Maharjan S *et al* 2021 Symbiotic photosynthetic oxygenation within 3D-bioprinted vascularized tissues *Matter* **4** 217–40
[57] Oh J-J, Ammu S, Vriend V D, Kieffer R, Kleiner F H, Balasubramanian S, Karana E, Masania K and Aubin-Tam M-E 2024 Growth, distribution, and photosynthesis of chlamydomonas reinhardtii in 3D hydrogels *Adv. Mater.* **36** 2305505
[58] Santabarbara S, Remelli W, Petrova A A and Casazza A P 2020 Influence of the wavelength of excitation and fluorescence emission detection on the estimation of fluorescence-based physiological parameters in different classes of photosynthetic organisms *Fluorescence Methods for Investigation of Living Cells and Microorganisms* (IntechOpen)
[59] Kabakova I, Zhang J, Xiang Y, Caponi S, Bilenca A, Guck J and Scarcelli G 2024 Brillouin microscopy *Nat. Rev. Method Primers* **4** 8
[60] Kabakova I, Scarcelli G and Yun S-H 2022 Chapter fifteen-Brillouin light scattering in biological systems *Semiconductors and Semimetals* (Elsevier)
[61] Bailey M, Correa N, Harding S, Stone N, Brasselet S and Palombo F 2020 Brillouin microspectroscopy data of tissue-mimicking gelatin hydrogels *Data Brief* **29** 105267
[62] Rioboó R J J, Gontán N, Sanderson D, Desco M and Gómez-Gaviro M V 2021 Brillouin spectroscopy: from biomedical research to new generation pathology diagnosis *Int. J. Mol. Sci.* **22** 8055
[63] Emig R, Zgierski-Johnston C M, Timmermann V, Taberner A J, Nash M P, Kohl P and Peyronnet R 2021 Passive myocardial mechanical properties: meaning, measurement, models *Biophys. Rev.* **13** 587–610
[64] Wu C, Zhang Y, Xu Y, Long L, Hu X, Zhang J and Wang Y 2023 Injectable polyaniline nanorods/alginate hydrogel with AAV9-mediated VEGF overexpression for myocardial infarction treatment *Biomaterials* **296** 122088
[65] Hassanpour P *et al* 2024 Mitochondria-loaded alginate-based hydrogel accelerated angiogenesis in a rat model of acute myocardial infarction *Int. J. Biol. Macromol.* **260** 129633
[66] Liu C, Wu Y, Yang H, Lu K, Zhang H, Wang Y, Wang J, Ruan L, Shen Z and Yu Q 2023 An injectable alginate/fibrin hydrogel encapsulated with cardiomyocytes and VEGF for myocardial infarction treatment *J. Mater. Sci. Technol.* **143** 198–206
[67] Wu Y, Chang T, Chen W, Wang X, Li J, Chen Y, Yu Y, Shen Z, Yu Q and Zhang Y 2021 Release of VEGF and BMP9 from injectable alginate based composite hydrogel for treatment of myocardial infarction *Bioact. Mater.* **6** 520–8
[68] Alonzo M, Kumar S A, Allen S, Delgado M, Alvarez-Primo F, Suggs L and Joddar B 2020 Hydrogel scaffolds with elasticity-mimicking embryonic substrates promote cardiac cellular network formation *Prog. Biomater.* **9** 125–37
[69] Mousavi A, Mashayekhan S, Baheiraei N and Pourjavadi A 2021 Biohybrid oxidized alginate/myocardial extracellular matrix injectable hydrogels with improved electromechanical properties for cardiac tissue engineering *Int. J. Biol. Macromol.* **180** 692–708
[70] Maiullari F *et al* 2018 A multi-cellular 3D bioprinting approach for vascularized heart tissue engineering based on HUVECs and iPSC-derived cardiomyocytes *Sci. Rep.* **8** 13532
[71] Bovone G, Dudaryeva O Y, Marco-Dufort B and Tibbitt M W 2021 Engineering hydrogel adhesion for biomedical applications via chemical design of the junction *ACS Biomater. Sci. Eng.* **7** 4048–76
[72] Han M, Zhang C and Ho S-H 2023 Immobilized microalgal system: an achievable idea for upgrading current microalgal wastewater treatment *Environ. Sci. Ecotechnol.* **14** 100227
[73] Spicer C D 2020 Hydrogel scaffolds for tissue engineering: the importance of polymer choice *Polym. Chem.* **11** 184–219
[74] Hayashi Y, Fujii T, Kim S, Badylak S F, D'Amore A and Wagner W R 2024 Intervening to preserve function in ischemic cardiomyopathy with a porous hydrogel and extracellular matrix composite in a rat myocardial infarction model *bioRxiv Preprint* (https://doi.org/10.1101/2024.07.02.601690) (posted onilne 04 July 2024)
[75] Gopalakrishnan A, Shankarappa S A and Rajanikant G K 2019 Hydrogel scaffolds: towards restitution of ischemic stroke-injured brain *Transl. Stroke Res.* **10** 1–18
[76] Song X, Wang X, Zhang J, Shen S, Yin W, Ye G, Wang L, Hou H and Qiu X 2021 A tunable self-healing ionic hydrogel with microscopic homogeneous conductivity as a cardiac patch for myocardial infarction repair *Biomaterials* **273** 120811

[77] Song X, Mei J, Ye G, Wang L, Ananth A, Yu L and Qiu X 2019 In situ pPy-modification of chitosan porous membrane from mussel shell as a cardiac patch to repair myocardial infarction *Appl. Mater. Today* **15** 87–99
[78] Fang J *et al* 2020 Injectable drug-releasing microporous annealed particle scaffolds for treating myocardial infarction *Adv. Funct. Mater.* **30** 2004307
[79] Vedadghavami A, Minooei F, Mohammadi M H, Khetani S, Rezaei Kolahchi A, Mashayekhan S and Sanati-Nezhad A 2017 Manufacturing of hydrogel biomaterials with controlled mechanical properties for tissue engineering applications *Acta Biomater.* **62** 42–63
[80] Vander Wiel J B, Mikulicz J D, Boysen M R, Hashemi N, Kalgren P, Nauman Levi M, Baetzold S J, Powell G G, He Q and Hashemi N 2017 Characterization of Chlorella vulgaris and Chlorella protothecoides using multi-pixel photon counters in a 3D focusing optofluidic system *RSC Adv.* **7** 4402–8
[81] Ferreira A S, Ferreira S S, Correia A, Vilanova M, Silva T H, Coimbra M A and Nunes C 2020 Reserve, structural and extracellular polysaccharides of Chlorella vulgaris: a holistic approach *Algal Res.* **45** 101757
[82] Wang M, Yin Z, Sun W, Zhong Q, Zhang Y and Zeng M 2023 Microalgae play a structuring role in food: effect of spirulina platensis on the rheological, gelling characteristics, and mechanical properties of soy protein isolate hydrogel *Food Hydrocoll.* **136** 108244
[83] Ng J Y, Chua M L, Zhang C, Hong S, Kumar Y, Gokhale R and Ee P L R 2020 Chlorella vulgaris extract as a serum replacement that enhances mammalian cell growth and protein expression *Front. Bioeng. Biotechnol.* **8** 564667
[84] Ojha N and Dhamoon A S 2023 *Myocardial Infarction, in StatPearls* (StatPearls Publishing)
[85] Dubois-Deruy E, Peugnet V, Turkieh A and Pinet F 2020 Oxidative stress in cardiovascular diseases *Antioxidants* **9** 32937950
[86] Chen H, Cheng Y, Tian J, Yang P, Zhang X, Chen Y, Hu Y and Wu J 2020 Dissolved oxygen from microalgae-gel patch promotes chronic wound healing in diabetes *Sci. Adv.* **6** eaba4311
[87] Fu Y, Xie X, Wang Y, Liu J, Zheng Z, Kaplan D L and Wang X 2021 Sustained photosynthesis and oxygen generation of microalgae-embedded silk fibroin hydrogels *ACS Biomater. Sci. Eng.* **7** 2734–44
[88] Rocha G S, Parrish C C and Espíndola E L G 2021 Effects of copper on photosynthetic and physiological parameters of a freshwater microalga (chlorophyceae) *Algal Res.* **54** 102223
[89] Farooq W, Naqvi S R, Sajid M, Shrivastav A and Kumar K 2022 Monitoring lipids profile, CO_2 fixation, and water recyclability for the economic viability of microalgae Chlorella vulgaris cultivation at different initial nitrogen *J. Biotechnol.* **345** 30–39
[90] McCauley J I, Ortega J S, Gentile C and Ralph P J 2022 Chapter 7-Microalgal applications in biomedicine and healthcare *Biomass, Biofuels, and Biochemicals* (Elsevier Online) (https://doi.org/10.1016/B978-0-323-96142-4.00012-9)
[91] Taghavi Takyar M B, Haghighat Khajavi S and Safari R 2019 Evaluation of antioxidant properties of Chlorella vulgaris and spirulina platensis and their application in order to extend the shelf life of rainbow trout (oncorhynchus mykiss) fillets during refrigerated storage *LWT* **100** 244–9